

# Combinatorial synthesis and characterization of a ternary epitaxial film of Co and Mn doped Ge (0 0 1)

F. Tsui<sup>a,\*</sup>, B.A. Collins<sup>a</sup>, L. He<sup>a</sup>, A. Mellnik<sup>a</sup>, Y. Zhong<sup>b</sup>, S. Vogt<sup>b</sup>, Y.S. Chu<sup>b</sup>

<sup>a</sup>Department of Physics and Astronomy, University of North Carolina, Chapel Hill, NC 27599, USA

<sup>b</sup>Advanced Photon Source, Argonne National Laboratory, Argonne, IL 60439, USA

Received 31 December 2006; accepted 30 May 2007

Available online 13 July 2007

## Abstract

We report combinatorial molecular beam epitaxy synthesis and properties of a ternary epitaxial film of Co and Mn co-doped Ge grown on Ge (0 0 1) substrate. Structural effects were examined in situ by reflection high-energy electron diffraction and ex situ by microbeam X-ray diffraction techniques, and magnetic properties were probed by using magneto-optic Kerr effect. Ternary epitaxial phase diagrams have been studied for total doping concentrations up to 30 at.%, where regions of coherent epitaxy and rough disordered growth and those of near room temperature ferromagnetic ordering have been identified.

© 2007 Elsevier B.V. All rights reserved.

**Keywords:** Epitaxial film; Magnetic semiconductor; Group IV semiconductor; Transition metal doping; Combinatorial thin film

## 1. Introduction

Advances in the synthesis of doped magnetic semiconductors have continued to enable a wide range of activities in the science and technology of spintronics. Recent publications [1,2] show that complementary doping using two transition metal dopants into Ge (0 0 1) lattice during molecular beam epitaxial (MBE) growth can stabilize epitaxial growth at significantly higher doping concentrations (as high as 15 at.%) than those from using a single dopant. It appears that using a dopant with a larger atomic radius than that of the Ge host in conjunction with a dopant with smaller atomic radius, at an appropriate atomic ratio between the two, can compensate for the internal stress caused by the individual dopants in the host lattice. Comprehensive studies of the ternary phase diagrams are needed, in order to explore interactions between the transition metal dopants beyond the effect of strain and, thus, enhance our ability to control synthesis and properties of this type of materials systems. The use of combinatorial approach is necessary for carrying out such studies of complex multi-component materials systems. Here, we present combinatorial

MBE synthesis and characterization of a ternary epitaxial system that contains transition metals, Co and Mn, co-doped into Ge (0 0 1) in the range of doping concentrations between 0 and 30 at.%.

## 2. Experiment

The ternary  $\text{Co}_x\text{Mn}_y\text{Ge}_{1-x-y}$  sample was grown on a semi-insulating Ge (0 0 1) substrate using combinatorial MBE techniques. The substrate was first cleaned using the standard RCA method, and then degassed at 600 °C under UHV conditions. A growth anneal cycle was employed to prepare a Ge (0 0 1) buffer layer of 380 Å thick, preceding the growth of the ternary combinatorial film. In each cycle, a thin Ge layer (typically 30–100 Å) was deposited at 250 °C and then annealed at 600 °C. The resulting surface is atomically smooth across the entire substrate with  $2 \times 1$  surface reconstructions, as determined by real-time scanning reflection high-energy electron diffraction (RHEED) measurements.

The ternary film was subsequently grown by sequential multilayer deposition of Ge, Co and Mn trilayers. Each trilayer consists of three submonolayer wedges, a Ge wedge with thicknesses from 1.6 to 2 Å, a Co wedge with thicknesses from 0 to 0.4 Å and a Mn wedge with thicknesses from 0 to 0.7 Å. Each element (wedge) is spread linearly over

\* Corresponding author. Tel.: +1 919 962 0305; fax: +1 919 962 0480.

E-mail address: [ftsui@physics.unc.edu](mailto:ftsui@physics.unc.edu) (F. Tsui).

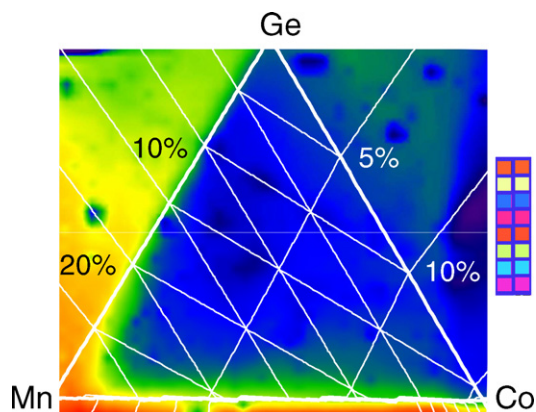


Fig. 1. (Color online) Specular reflectance at 658 nm of the  $\text{Co}_x\text{Mn}_y\text{Ge}_{1-x-y}$  (0 0 1) combinatorial film with a nominal thickness of 500 Å. It was taken over a 2D mesh with spacing of  $100\ \mu\text{m} \times 100\ \mu\text{m}$  using a diode laser focused to a FWHM of  $100\ \mu\text{m}$ . The composition and the corresponding grid are determined by microbeam XRF measurements. Warm colors correspond to high reflectance and cold colors correspond to low reflectance. The range of reflectance shown is between 100% (red) and 80% (dark blue). The height of the image is 5 mm. The substrate is much larger than the region shown, and the sample is broken near the top of the image (not shown).

a lateral distance of 5 mm along a direction that is  $120^\circ$  rotated from the other two, creating a triangular region of the sample containing all three elements. The thicknesses expressed here are in Ge equivalent values, i.e. converted to the same atomic density as Ge matrix rather than the native metallic matrices for the two transition metals. The resulting concentration range for Co ( $x$ ) is between 0 and 17 at.%, and the corresponding values for Mn ( $y$ ) are 0 and 29 at.%. A triangular shaped shadow mask [3] was used in combination with pneumatic source shutters and real-time atomic absorption spectroscopy flux monitors to control the thickness profiles of the three elements and, thus, the composition profile across the substrate. To illustrate the physical extent of the ternary sample, a specular reflectance image is shown in Fig. 1. Ge and Co were evaporated from electron beam hearths and Mn flux was from an effusion cell. The growth rates were maintained at  $\sim 0.1\ \text{\AA/s}$ , at a substrate temperature of  $250\ ^\circ\text{C}$  and a base pressure of  $\sim 10^{-10}$  Torr. The sample was terminated with a Ge layer (25 Å) and followed by a post-growth anneal at  $450\ ^\circ\text{C}$ . The nominal film thickness is 500 Å.

Magnetic properties were examined ex situ using magneto-optic Kerr effect (MOKE). A diode laser at a wavelength of 658 nm was used to perform longitudinal MOKE at near normal incidence (incident angle about  $15^\circ$  from normal). The full width at half maximum (FWHM) of the laser spot was focused to about  $100\ \mu\text{m}$  in diameter at the sample, which corresponds to a compositional variation of  $<0.5$  at.% within the laser spot. A precision translation stage was used to scan the sample with respect to the laser. The MOKE signal was modulated using a photoelastic modulator, and the Kerr rotation and dichroism signal were detected separately via lock-in amplifiers. The DC specular reflectance signal was also collected, as shown in Fig. 1. A Joule–Thomson refrigerator mounted on the translation stage between the pole pieces of an

electromagnet was used to vary sample temperature between 78 and 590 K.

Composition and structural properties were studied using X-ray microbeam techniques at the 2-BM beamline of the Advanced Photon Source (APS) at Argonne National Laboratory. Both microbeam X-ray diffraction (XRD) and X-ray fluorescence spectroscopy (XRF) techniques were used. A micron-sized X-ray beam ( $\sim 10\ \mu\text{m}$  in lateral dimensions) was scanned across the sample, using a precision sample-stage mounted at the center of a Huber 4-circle diffractometer. The spot size of the X-ray beam was about  $10^3$  times smaller than the ternary sample, which corresponds to a compositional variation of  $<0.05$  at.% within the beam. The latter value is adequately small even with a modest spreading of the beam on the sample owing to different diffraction conditions, i.e. different incident angles. Both out-of-plane XRD measurements along [0 0 L] and 2D reciprocal space mapping in the (HKL) plane were carried out through various reflections, including (0 0 4) and (1 1 3).

In addition to a point detector for high resolution XRD experiments, an area detector (CCD with  $2048\ \text{pixels} \times 3072\ \text{pixels}$ ) was also used for powder XRD experiments. The area detector enables simultaneous detection of scattering intensities within a relatively large region of reciprocal space, thus, enhancing sensitivity to intensities from certain types of disorders. The CCD was first aligned to the substrate using the Bragg reflections and then positioned to cut through the features in reciprocal space, such as the twinned {0 2 2} reflections resulting from stacking faults along  $\langle 1\ 1\ 1 \rangle$ . The  $2\theta$  values for the CCD images were calibrated using a  $\text{CeO}_2$  NIST powder diffraction standard. An energy-dispersive fluorescence detector was used for the XRF measurements to quantify the amount of Co and Mn in the sample (composition grid in Fig. 1) using calibrated references, and it was also used to determine film composition during XRD experiments.

Both 2D mesh scans, typically a  $100\ \mu\text{m} \times 100\ \mu\text{m}$  grid over the entire sample or regions of interest, and line scans were used to probe the composition dependence, including XRD, XRF and MOKE experiments.

### 3. Results and discussion

The specular reflectance for the ternary region of the  $\text{Co}_x\text{Mn}_y\text{Ge}_{1-x-y}$  (0 0 1) epitaxial film is in general lower than that of the binary regions of the film, as shown in Fig. 1, and is comparable to that of the bare substrate. In particular, the binary  $\text{Mn}_y\text{Ge}_{1-y}$  portion of the film exhibits high specular reflectance indicative of metallic alloys, such as the  $\text{Co}_x\text{Mn}_y$  binary alloys (shown at the bottom of Fig. 1). The amount of diffusive scattering at this wavelength is low and nearly uniform across the sample, excluding various extrinsic macroscopic flaws (e.g. pits) on the sample (the dark spots in Fig. 1). The qualitatively low specular reflectance of the ternary region with respect to the binary counterparts provides not only a convenient means for positioning the sample, but also a strong evidence that a large of portion of the ternary film is semiconducting.

The crystalline properties of the film exhibit distinctive composition dependent regions, as determined by XRD

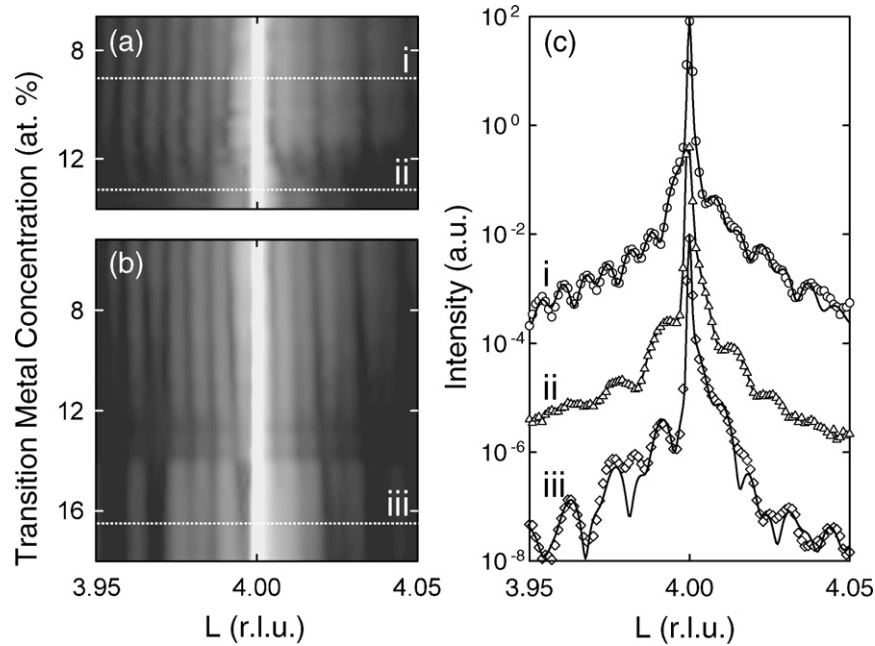


Fig. 2. Evolution of XRD intensities of the  $\text{Co}_x\text{Mn}_y\text{Ge}_{1-x-y}$  (0 0 1) epitaxial film along the [0 0 L] direction through the Ge (0 0 4) reflection as a function of composition. (a and b) CTR intensities in logarithmic scale along L, the reciprocal lattice units normal to the surface (horizontal axis) vs. total transition metal concentration ( $x + y$ ) in at. % (vertical axis) for two Co to Mn atomic ratios,  $x/y = 3:1$  and  $1:5$ , respectively. The dashed lines correspond to the intensities shown in (c). (c) Three characteristic CTR intensities along [0 0 L] at various doping concentrations. For clarity the three scans are shifted by two decades vertically with respect to each other. Lines over the points for (i) and (iii) are fits using a kinematical model discussed in the text, and the line for (ii) behind the points (triangles) is for connecting the points to guide the eyes.

experiments using crystal truncation rod (CTR) analysis. In order to illustrate the characteristic composition dependence, 0 0 L CTR intensities across the ternary sample at two fixed values of Co to Mn atomic ratios are shown in Fig. 2. At low doping concentrations, the CTR intensities exhibit interference fringes on either side of the (0 0 4) Bragg reflection with regular spacings in L [trace (i) in Fig. 2(c)], and the intensity fringes shift in L systematically with increasing doping concentration. As transition metal concentration increases, the observed behavior for Co-rich doping differs qualitatively from the Mn-rich counterparts: the fringe patterns for the former disappear at high doping concentrations [above  $\sim 12$  at. % in Fig. 2(a) and trace (ii) in Fig. 2(c)]; in contrast the behavior for the latter “lingers-on” but the spacings become increasingly irregular [above  $\sim 14$  at. % in Fig. 2(b) and trace (iii) in Fig. 2(c)].

The observed fringe patterns arise from coherent interference between the scattered X-rays from the atomic planes in the substrate, the film, and the interfaces. Since the Bragg reflections from the film are dominated by the intensities from the Ge substrate, intensities of the fringe patterns become the primary source for examining the coherent structural properties of the film, including surface and interfacial qualities, strain states and number of atomic layers—film thickness. The presence of regular fringes in L provides a strong indication that the film has an atomically smooth surface and is coherent with respect to the substrate. The spacing of the fringes is related to the film thickness, and their phase and the corresponding shift in L are the result of lattice mismatch between the atomic layers of the film and the substrate. The observed behavior is evidently the result of coherent 2D epitaxial growth, and the

disappearance of the fringe patterns indicates the presence of a roughening transition from coherent 2D to rough 3D growth. This observation is consistent with previous studies [2] using binary combinatorial samples that show the presence of a thickness dependent 2D to 3D roughening transition as a function of doping concentration. In contrast, the effect associated with the observed transition to irregularly spaced fringe patterns in the Mn-rich region of the sample is perhaps a bit subtle, but the most likely candidate for such an effect is that the film becomes less homogeneous in its composition while still remains 2D like. The inhomogeneity can give rise to additional characteristic length scales and corresponding Fourier components that complicate the interference patterns.

In order to examine and quantify the structural properties within the coherent 2D growth regime, the diffraction intensities have been analyzed using to a simple kinematical model [4] given by

$$I \propto \left| \frac{1}{[1 - \exp(-iq_z a)]} + \sum_{n=0}^{N-1} \exp(inq_z d) \right|^2. \quad (1)$$

Here  $q_z$  is the out-of-plane component of scattering vector  $\mathbf{q}$ ,  $a$  and  $d$  the respective out-of-plane lattice parameters of the substrate and the film and  $N$  is total number of atomic layers. The two terms within the modular square in Eq. (1) are the scattering amplitudes of the substrate and the film, respectively. By fitting the measured diffraction intensities, structural parameters have been determined quantitatively. The fitting function used for the analysis consists of terms associated with the substrate, interface, the buffer and the film, whose parameters

include number of atomic layers, Debye–Waller factor, and the out-of-plane lattice constant, in addition to a Voigt background function representing the diffusive scattering from the Bragg reflection of the substrate. A more detailed description of the CTR analysis is published elsewhere [5]. The diffraction intensities at every measured point on the sample (a mesh) were fit iteratively from one point to the next.

An example of a good fit within the coherent 2D growth regime is shown in the line (i) in Fig. 2(c). When the film roughens with a 3D surface, the fringes disappear [intensity (ii) in Fig. 2(c)] and the diffraction intensity can no longer be fit to a simple model. When the fringe patterns become irregular, it is also difficult to obtain a good fit [the line (iii) in Fig. 2(c)] without introducing additional parameters associated with possible compositional inhomogeneity. The behavior of the more complex structures can certainly be modeled and quantified if the nature and the spatial extent of the inhomogeneity are elucidated. To that end complementary experiments that are sensitive to these effects are being carried out, including scanning transmission electron microscopy/spectroscopy and local electrode atom probe tomography.

XRD intensities away from the Bragg reflections also exhibit distinctive composition dependent regions correspondingly, as examined by using an area detector (CCD) in order to increase the throughput of the measurement for certain disorders. The characteristic diffraction patterns are shown in Fig. 3. As discussed above, the CCD was first aligned to the substrate using Bragg reflections, and then positioned to sample the reciprocal coordinates away from the Bragg reflections of the substrate, searching for weak diffraction signals from disorder and secondary phases, including those from stacking faults and powder. At low doping concentrations within the coherent 2D growth regime, the XRD intensities are nearly featureless, as shown in Fig. 3(a) except for a diffused X-shaped pattern from the thermal diffuse scattering (TDS) of the substrate. Above the concentration where the 2D to 3D roughening transition takes place, intensities from the twinned  $\{0\ 2\ 2\}$  reflections appear, as shown in the bright spots in Fig. 3(b). The formation of the  $60^\circ$  twins with respect to the  $\langle 1\ 1\ 1 \rangle$  directions is evidently the result of stacking faults formed during the rough 3D growth along the same directions. It is well known that low temperature MBE growth of Si and Ge is prone to the formation of stacking faults along  $\langle 1\ 1\ 1 \rangle$  and the corresponding  $60^\circ$  twins [6].

At the Mn-rich portion of the sample (especially along the binary  $\text{Mn}_y\text{Ge}_{1-y}$  edge), as transition metal concentration increases above the concentration where the CTR fringe patterns around the Bragg reflections become highly irregular [Fig. 2(b and c)], textured powder intensities start to emerge, as shown in Fig. 3(c and d). The powder intensities from the CCD were first integrated at constant values of  $2\theta$  and then fit to a Gaussian function. The resulting powder diffraction patterns (the intensities and  $2\theta$  values) are consistent with those from textured Mn and  $\text{MnO}_2$  precipitates. The only region where powder intensities are detected is along the binary  $\text{Mn}_y\text{Ge}_{1-y}$  for Mn concentration above 10 at.%, and the region widens into the ternary above 15 at.%. This is consistent with recent reports [7,8] that Mn has a strong tendency to form Mn-rich regions

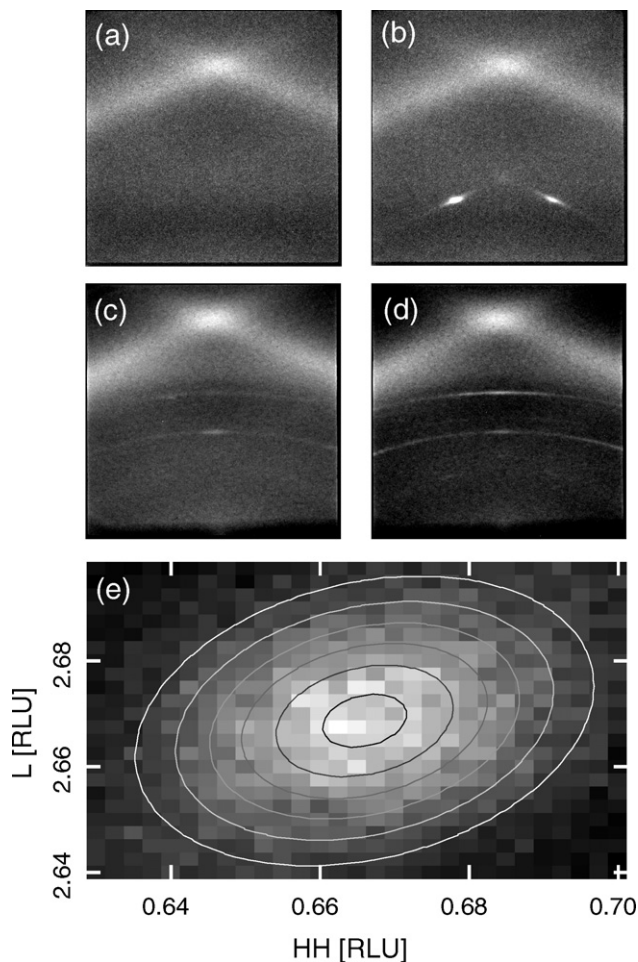


Fig. 3. 2D XRD patterns taken at various regions of composition, (a–d) using an area detector (CCD images), and (e) using a point detector via high resolution XRD reciprocal space mapping. The plane in reciprocal space is defined by  $[H\ H\ 0]$  vs.  $[0\ 0\ L]$ . (a) 2D growth region at low transition metal concentration. (b) Co-rich 3D rough growth region. (c) and (d)  $\text{Mn}_y\text{Ge}_{1-y}$  binary region with respective Mn concentrations of  $\sim 15$  and  $\sim 20$  at.%. (e) A high resolution reciprocal space map around the  $(2/3, 2/3, 8/3)$  stacking fault peak in the Co-rich 3D growth region, with Co and Mn concentrations at 8.0 and 7.2 at.%, respectively. The elliptical contours are from a 2D Gaussian fit.

and/or precipitates in Ge. The powder intensities drop precipitously as Co is being added as a second dopant. This indicates the critical role played by Co in suppressing Mn precipitation and stabilizing atomic species of Mn in Ge, consistent with recent first principle calculations [9,10] that show an increase in energy for the formation of Mn clusters in the presence of Co ions.

In addition to the CCD Images, lattice parameters and symmetry of the stacking faults have been examined using 2D reciprocal space mapping with a narrow slit point detector, as shown in Fig. 3(e). Near the onset of the 3D roughening transition, the twinned  $\{0\ 2\ 2\}$  reflections are nearly lattice matched with the Ge substrate. As the stacking fault intensity increases, the peak position in  $L$  also increases, while the position in  $HH$  decreases, indicating the presence of an increasingly large out-of-plane tetragonal distortion. The observed distortion does not appear to be the result of coherent epitaxy, since the latter would require the in-plane component

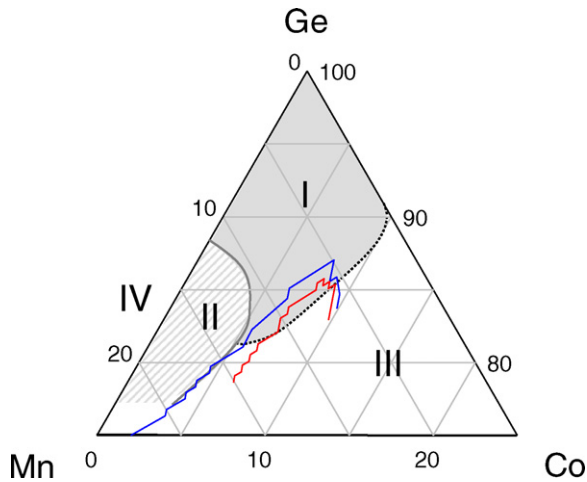


Fig. 4. (Color online) Structural and magnetic phase diagrams of the  $\text{Co}_x\text{Mn}_y\text{Ge}_{1-x-y}$  (0 0 1) epitaxial film with a nominal thickness of 500 Å. Various structures, as identified by the XRD experiments discussed in the text, are labeled as numbers I–IV. The two color contour lines indicate the  $T_C$  boundaries as a function of composition determined by MOKE experiments, red line: 300 K and blue line: 250 K.

to remain constant. A similar effect has been observed in Co and Fe co-doped Ge (0 0 1) epitaxial films [11]; however, its origin is unclear at this point.

Based on the XRD analysis, an epitaxial phase diagram has been obtained identifying various composition dependent growth modes, as shown in Fig. 4. The region, where the XRD intensities exhibit coherent interference fringes, is identified by the CTR analysis as the region of coherent 2D growth (region I). The Mn-rich region with complex irregular XRD fringes is identified as quasi 2D growth (region II), owing to possible compositional inhomogeneity and the detection of Mn precipitates within its boundary by CCD. The Co-rich region at high doping concentrations is determined to be the region of rough 3D growth (region III), where the CTR interference fringes disappear and stacking fault and  $60^\circ$  twins appear. There are no detectable stacking faults or twins in regions I and II. Trace amounts of Mn precipitates have been detected in the predominantly binary region of Mn and Ge (region IV), which also extends into part of region II at high Mn concentrations. A more detailed phase diagram that contains structural parameters from the fits, e.g. strain states and disorders, will be published elsewhere.

Also shown in Fig. 4 are two contours of Curie temperatures versus composition, as determined by MOKE measurements. The phase diagrams demonstrate that there is a region where coherent 2D epitaxial growth and high

temperature ferromagnetism coexist. This finding offers exciting prospects for exploring promising materials candidates for spintronics.

#### 4. Summary

Combinatorial MBE synthesis and properties of a ternary epitaxial film of  $\text{Co}_x\text{Mn}_y\text{Ge}_{1-x-y}$  grown on Ge (0 0 1) substrate have been studied. Ternary epitaxial phase diagrams have been examined using microbeam X-ray techniques and MOKE measurements for total doping concentrations up to 30 at.%. Composition dependent regions of coherent epitaxy and rough disordered growth and those of near room temperature ferromagnetic ordering have been identified.

#### Acknowledgements

We thank P. Muduli and W. Rice for assistance and discussions, and Q. Shen at APS for support. The work was supported in part by US DOE/BES DE-FG02-05ER46216 for characterization and for student support, by US NSF DMR-0441218, and by DOD W911NF-05-1-0173 for MBE instrumentation. An APS subcontract 5F-00428 for partial student support is also acknowledged. BAC wishes to thank the 8th National School on Neutron and X-ray Scattering. Use of the Advanced Photon Source is supported by the US Department of Energy, Office of Sciences, Office of Basic Energy Sciences, under contract no. DE-AC02-06CH11357.

#### References

- [1] F. Tsui, L. He, L. Ma, A. Tkachuk, Y.S. Chu, K. Nakajima, T. Chikyow, Phys. Rev. Lett. 91 (2003) 177203.
- [2] F. Tsui, L. He, A. Tkachuk, S. Vogt, Y.S. Chu, Phys. Rev. B 69 (2004) 081304R.
- [3] F. Tsui, L. He, Rev. Sci. Instrum. 76 (2005) 062206.
- [4] I.K. Robinson, Rep. Prog. Phys. 55 (1992) 599–651.
- [5] Y.S. Chu, Y. Zhong, B.A. Collins, F. Tsui, Appl. Surf. Sci. 254 (2007) 714.
- [6] O.P. Karpenko, S.M. Yalisove, D.J. Eaglesham, J. Appl. Phys. 82 (1997) 1157.
- [7] S. Sugahara, K.L. Lee, S. Yada, M. Tanaka, Japan J. Appl. Phys. 44 (2005) L1426.
- [8] D. Bougeard, S. Ahlers, A. Trampert, N. Sircar, G. Abstreiter, Phys. Rev. Lett. 97 (2006) 237202.
- [9] A. Continenza, G. Profeta, S. Picozzi, Phys. Rev. B 73 (2006) 035212.
- [10] A. Continenza, G. Profeta, S. Picozzi, Appl. Phys. Lett. 89 (2006) 202510.
- [11] L. He, B.A. Collins, F. Tsui, Y. Zhong, S. Vogt, Y.S. Chu, J. Vac. Sci. Tech. B 25 (2007) 1217.